Journal of Medicinal Chemistry

ARTICLE

pubs.acs.org/jmc

Fine-Tuning the Selectivity of Aldosterone Synthase Inhibitors: Structure−Activity and Structure−Selectivity Insights from Studies of Heteroaryl Substituted 1,2,5,6-Tetrahydropyrrolo[3,2,1-*ij*]quinolin-4-one Derivatives

Simon Lucas,[†,§] Matthias Negri,[†] Ralf Heim,[†] Christina Zimmer,[†] and Rolf W. Hartmann*[,†,‡]

[†]Pharmaceutical and Medicinal Chemistry, Saarland University, Campus C2.3, D-66123 Saarbrücken, Germany

[‡]Helmholtz Institute for Pharmaceutical Research Saarland (HIPS), Campus C2.3, D-66123 Saarbrücken, Germany

Supporting Information

ABSTRACT:

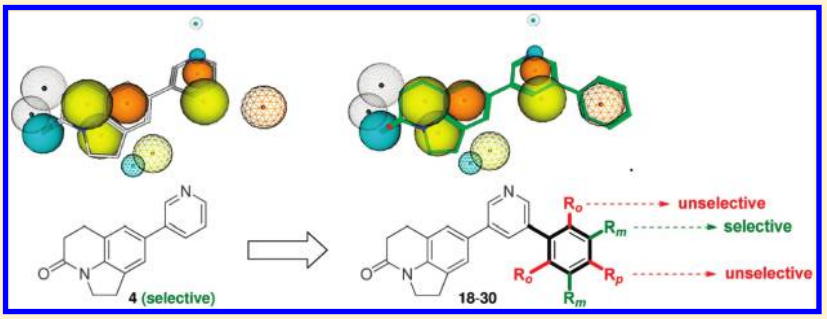

Pyridine substituted 3,4-dihydro-1*H*-quinolin-2-ones (e.g., **1**−**3**) constitute a class of highly potent and selective inhibitors of aldosterone synthase (CYP11B2), a promising target for the treatment of hyperaldosteronism, congestive heart failure, and myocardial fibrosis. Among these, ethyl-substituted **3** possesses high selectivity against CYP1A2. Rigidification of **3** by incorporation of the ethyl group into a 5- or 6-membered ring affords compounds with a pyrroloquinolinone or pyridoquinolinone molecular scaffold (e.g., **4** and **5**). It was found that these molecules are even more potent and selective CYP11B2 inhibitors than their corresponding open-chain analogues. Moreover, pyrroloquinolinone **4** exhibits no inhibition of the six most important hepatic CYP enzymes as well as a bioavailability in the range of the marketed drug fadrozole. The SAR studies disclose that subtle changes in the heterocyclic moiety are responsible for either a strong or a weak inhibition of the highly homologous 11β-hydroxylase (CYP11B1). These results are not only important for fine-tuning the selectivity of CYP11B2 inhibitors but also for the development of selective CYP11B1 inhibitors that are of interest for the treatment of Cushing's syndrome and metabolic syndrome.

INTRODUCTION

Congestive heart failure (CHF) is a condition of insufficient cardiac output and reduced systemic blood flow, which provokes a chronic activation of the renin−angiotensin−aldosterone system (RAAS). As a consequence, the excessive release of angiotensin II (Ang II) and aldosterone leads to an increased blood pressure and to a further deterioration of heart function, mainly mediated via epithelial sodium retention by mineralocorticoid receptor (MR) activation as well as Ang II mediated vasoconstriction.[1] Moreover, aldosterone is known to exert direct effects on the heart. Activation of nonepithelial MRs stimulates the progressive synthesis and deposition of fibrillar collagens in fibroblasts and results in myocardial fibrosis.[2] Until today, various drug classes targeting the RAAS have been developed in order to interrupt the circle of chronic neurohormonal activation, acting either by inhibition of the key regulator enzymes or by blocking the actions of the effector hormones by functional antagonism, affording a successful treatment of heart failure and hypertension. Inhibitors of the angiotensin converting enzyme (ACE) proved to trigger a down-regulation of circulating aldosterone, but increased levels of aldosterone may be seen after several months of therapy, presumably due to potassium stimulated secretion.[3] The persistence of aldosterone secretion despite treatment with ACE inhibitors and the evidence of the deleterious effects of aldosterone on cardiovascular function led to the assumption that blocking the mineralocorticoid receptor might provide additional benefit. This hypothesis has been corroborated in two recent clinical trials by using the MR antagonists spironolactone and eplerenone in addition to the standard

Received: November 16, 2010
Published: March 08, 2011

Chart 1. CYP11B2 Catalyzed Biosynthesis of Aldosterone

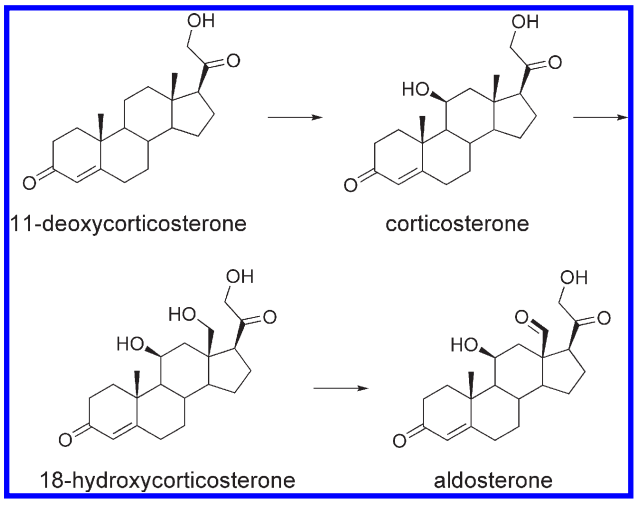

Chart 2. Title Compounds

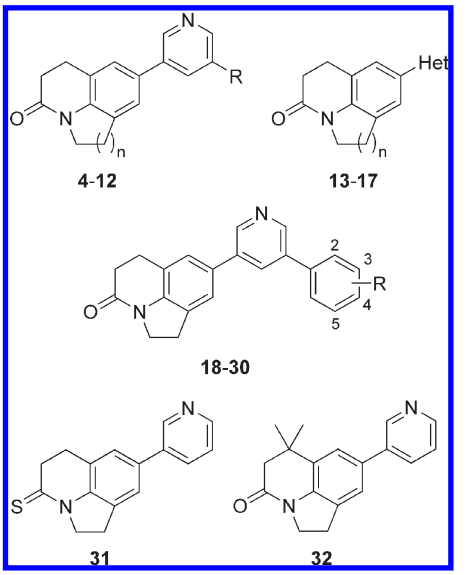

therapy of patients with chronic congestive heart failure and in patients after myocardial infarction, respectively.[4] Aldosterone antagonistic therapy, however, raises several issues. Spironolactone can induce severe side effects due to its low selectivity against other steroid hormone receptors.[4,5] Although eplerenone is more selective, clinically relevant hyperkalemia remains a principal therapeutic risk.[6] Moreover, the elevated plasma aldosterone concentrations are left unaffected on a pathological level, promoting the up-regulation of MR expression[7] and nongenomic aldosterone effects[8] on the insufficient heart.

Hence, we hypothesized a novel approach for the treatment of hyperaldosteronism, congestive heart failure, and myocardial fibrosis by lowering the elevated plasma aldosterone levels via blockade of aldosterone synthase (CYP11B2), the key enzyme of mineralocorticoid biosynthesis.[9,10] Inhibition of steroidogenic CYP enzymes had earlier been demonstrated to be very efficient for the treatment of steroid hormone dependent diseases. Aromatase (CYP19) and 17α-hydroxylase/17,20-lyase (CYP17) inhibitors are first-line or upcoming therapeutics for the treatment of breast or prostate cancer, respectively. Our drug design efforts against CYP11B2 are based on our long-standing experience in the development of CYP19[11] and CYP17[12] inhibitors. CYP11B2 is a mitochondrial cytochrome P450 enzyme localized mainly in the zona glomerulosa of the adrenal gland. It catalyzes the terminal three oxidation steps in the biogenesis of aldosterone in humans via initial hydroxylation of 11-deoxycorticosterone at 11β-position to yield corticosterone, followed by two subsequent hydroxylations at C_{18} and water release to yield aldosterone (Chart 1).[13] In addition to the potential therapeutic utility in cardiovascular diseases, radiolabeled inhibitors of this enzyme might be a useful tool for molecular imaging of CYP11B expression in adrenocortical tissue and thus for the diagnosis of adrenal tumors.[14] Because of selectively binding to CYP11B2, these compounds are also interesting for the imaging of Conn adenomas, which are characterized by high expression of CYP11B2.[15]

A critical issue in the development of CYP11B2 inhibitors is to accomplish selectivity against other cytochrome P450 (CYP) enzymes because the characteristic complexation of the heme iron is likely to occur in other CYP enzymes, too. The selectivity issue becomes especially critical with respect to 11β-hydroxylase (CYP11B1), the key enzyme of glucocorticoid biosynthesis, highly homologous to CYP11B2.[16] Consequent structural optimization of a hit discovered by compound library screening performed in our laboratory led to a series of nonsteroidal aldosterone synthase inhibitors with high selectivity against other cytochrome P450s.[17,18] However, several potent and selective compounds, mostly pyridine-substituted naphthalenes[19,20] and dihydronaphthalenes,[21] still showed a strong inhibition of the hepatic drug metabolizing enzyme CYP1A2 and no inhibitory effect on the aldosterone biosynthesis in vivo.

Currently, no crystal structure of CYP11B enzymes exist, which could assist in solving ligand-binding and mechanistic issues. However, various groups have developed homology models of CYP11B1 and CYP11B2 in the past decade,[18,22] focusing on different aspects in the generation of the models and integrating most of the mutational studies from the literature. All the published models were built upon bacterial templates and hepatic CYPs. Furthermore, two pharmacophore models have been developed, both successfully applied in a ligand-based drug design approach.[20,23] In the present study, we describe the development of 1,2,5,6-tetrahydropyrrolo[3,2,1-*ij*]quinolin-4-ones and structurally related aldosterone synthase inhibitors (Chart 2) starting from the previously described inhibitors **1**−**3** (Chart 3). A multitemplate homology model was generated using the crystal structures of five human CYPs as templates to assist the design of the molecules. The novelty of this approach consists in the use of the steroidogenic CYP19 enzyme, combined with selected segments taken from other CYPs. Moreover, we also extended our CYP11B2-pharmacophore model enlarging the structural diversity of the data set. Finally, potent aldosterone synthase inhibitors were found with improved selectivity against the cognate CYP11B1, the steroidogenic enzymes CYP17 (17α-hydroxylase/C17,20-lyase) and CYP19 (aromatase), as well as the six most important drug-metabolizing CYPs (CYP1A2, CYP2B6, CYP2C9, CYP2C19, CYP2D6, and CYP3A4). The in vivo pharmacokinetic profiles of some promising compounds were determined in male Wistar rats.

Chart 3. Considerations Leading to Compounds 4 and 5

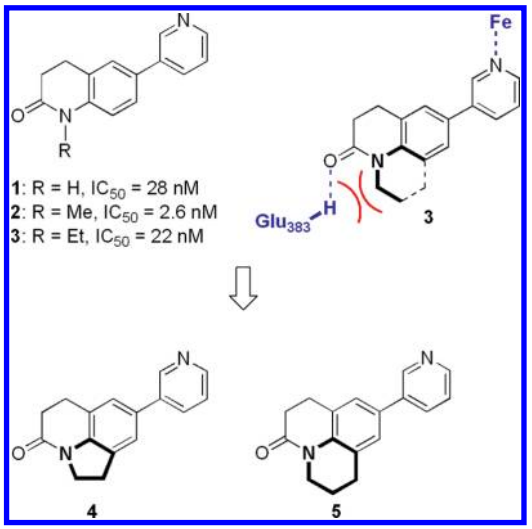

CHEMISTRY

The key synthetic transformation leading to the target compounds was a Suzuki coupling to connect the pyrrolo- or pyridoquinolinone scaffold to various *N*-heterocyclic systems, in most cases a derivative of 3-pyridine (Scheme 1). The advanced intermediates **4a** and **5a** as well as **32a** were prepared in three consecutive steps starting from commercially available indoline or 1,2,3,4-tetrahydroquinoline as the initial building block. The sequence of amide formation and subsequent Friedel−Crafts cyclization to afford **4b** and **5b** has been described previously and was also used for the synthesis of the *gem*-dimethyl analogue **32a**.[24] Regioselective bromination was accomplished by treating the fused heterocycles with *N*-bromosuccinimide in DMF at 0 °C. The pyrrolo- or pyridoquinolinones **4**−**7**, **13**−**16**, and **32** were obtained by Suzuki coupling of the arylbromides **4a**, **5a**, or **32a** with an *N*-heterocyclic boronic acid.[25] Copper catalyzed *N*-arylation of **4a** with imidazole gave rise to the 1-imidazolyl derivative **17**.[26] Alternatively, the bromo-substituted pyrroloquinolinone **4a** was transformed into the corresponding pinacol boronate **6a** by treating with bis-(pinacolato)diboron under palladium catalysis[27] and was subsequently used for cross-coupling with a derivative of 3-bromopyridine to afford compounds **8**−**12** and **18**−**30**. If not commercially available, the 3-bromopyridines used in this step were prepared as outlined in Scheme 2 either from 3-bromo-5-methoxypyridine by demethylation and subsequent alkylation (**8a**, **9a**) or from 3,5-dibromopyridine by Suzuki coupling with a substituted arylboronic acid (**19a**−**30a**). The hydroxypyridine **10** was synthesized by treating the corresponding methoxy derivative **6** with concentrated hydrobromic acid under reflux. Thionation of pyrroloquinolinone **4** with Lawessons reagent in dry toluene afforded the thio-analogue **31**.

MOLECULAR MODELING

Despite a very low sequence identity (<25%), all structures of cytochrome P450s known so far show a very similar tertiary fold with the same number of α-helixes (A−L) and β-sheets (10).[28] Moreover, they present several common and flexible structural features like B/C-loop and F/G segment (F helix, F/G loop, G helix), characterized by a pronounced flexibility that control the access to the CYP active site and its volume. The F/G-segment forms both roof and one side of the active site, and it is placed perpendicular to the I-helix and opposite to the heme. The I-helix

Scheme 1[a]

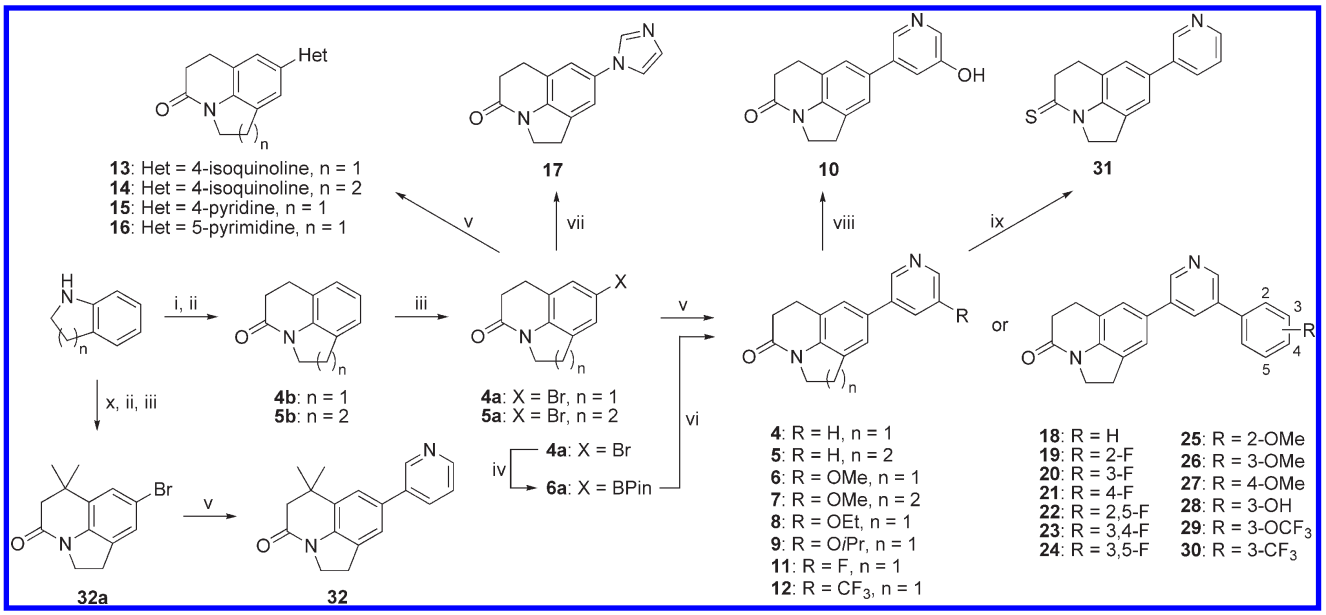

[a] Reagents and conditions: (i) 3-chloropropanoyl chloride, acetone, reflux; (ii) $AlCl_3$, NaCl, 150 °C; (iii) NBS, DMF, 0 °C; (iv) bis(pinacolato)diboron, $Pd(dppf)Cl_2$, KOAc, DMSO, 80 °C; (v) heteroarylboronic acid, $Pd(PPh_3)_4$, aq $NaHCO_3$, DMF, μw, 150 °C or heteroarylboronic acid, $Pd(PPh_3)_4$, aq Na_2CO_3, toluene/ethanol, reflux; (vi) heteroarylbromide, $Pd(PPh_3)_4$, aq Na_2CO_3, toluene/ethanol, reflux; (vii) imidazole, Cu_2SO_4, K_2CO_3, 180 °C; (viii) conc HBr, reflux; (ix) Lawessons reagent, toluene, reflux; (x) 3,3-dimethylacryloylchloride, acetone reflux (Het = heteroaryl, BPin = pinacol boronate).

dx.doi.org/10.1021/jm101470k | J. Med. Chem. 2011, 54, 2307–2319

Scheme 2[a]

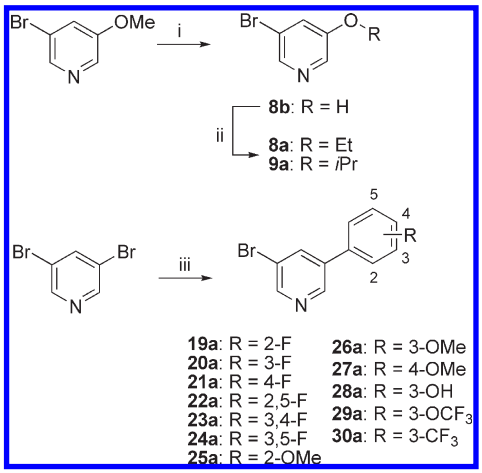

[a] Reagents and conditions: (i) conc HBr, reflux; (ii) alkylhalide, K_2CO_3, DMF, rt; (iii) arylboronic acid, $Pd(PPh_3)_4$, aq Na_2CO_3, toluene/ethanol, reflux.

extends through the whole enzyme and presents a kink close to a highly conserved acidic residue (Asp317), the catalytic Thr318, and the heme group. Human CYP11B1 and CYP11B2 differ only in 32 amino acids out of 503 (93% sequence identity).[29] However, a variety of amino acid mutations spread throughout CYP11B1 and CYP11B2 are known to modulate enzyme functionalities. Moreover, residue swapping experiments,[30] in which CYP11B1 residues were exchanged with their CYP11B2 counterparts and vice versa, suggest that amino acids that are part of the I-helix lining the active site and the *N*-terminal region of the CYP11B enzymes contribute most significantly to changes in catalytic activities. Very recently, the crystal structure of the human CYP19 enzyme has been resolved (PDB entry 3eqm).[31] It represents a very promising template for CYP11B1 and CYP11B2 models because active site similarities (hot spots) are feasible considering the scaffold similarity of the substrates and the potent "dual-inhibitor" profiles (CYP11B2 and CYP19) seen for many potent CYP11B inhibitors (e.g., fadrozole, compound **33**). Thus, a multitemplate strategy was followed to build a set of homology models of CYP11B2 using the crystal structures of human CYP19, CYP1A2, CYP2E1, CYP2C9, and CYP2D6 as templates. CYP19, CYP2C9, and CYP3A4 have been trialed out as core template, necessary for a correct alignment of all the different CYPs, with CYP2C9 resulting the most appropriate one. Successively, regions of CYP2C9 with a low sequence identity to CYP11B2 were exchanged with fragments from other CYPs showing a much higher degree of similarity. When no high similarity could be achieved, more templates were selected. Intersection regions between different crystal structures were also based on two or more templates. Finally, the sequence identity between CYP11B2 and the "patchwork" alignment was improved from ca. 23% (with respect to the single CYPs) to ca. 45%. Important criteria in the choice of the fragments were mutagenesis information (special attention was given to residues that are important for aldosterone synthase function) as well as ligand-steered considerations (i.e., ligands of CYP2E1 with isoquinoline substructures were included in model generation due to structural similarity to a series of highly potent isoquinoline substituted derivatives[20,32] developed in our laboratory). The final models were validated by docking a series

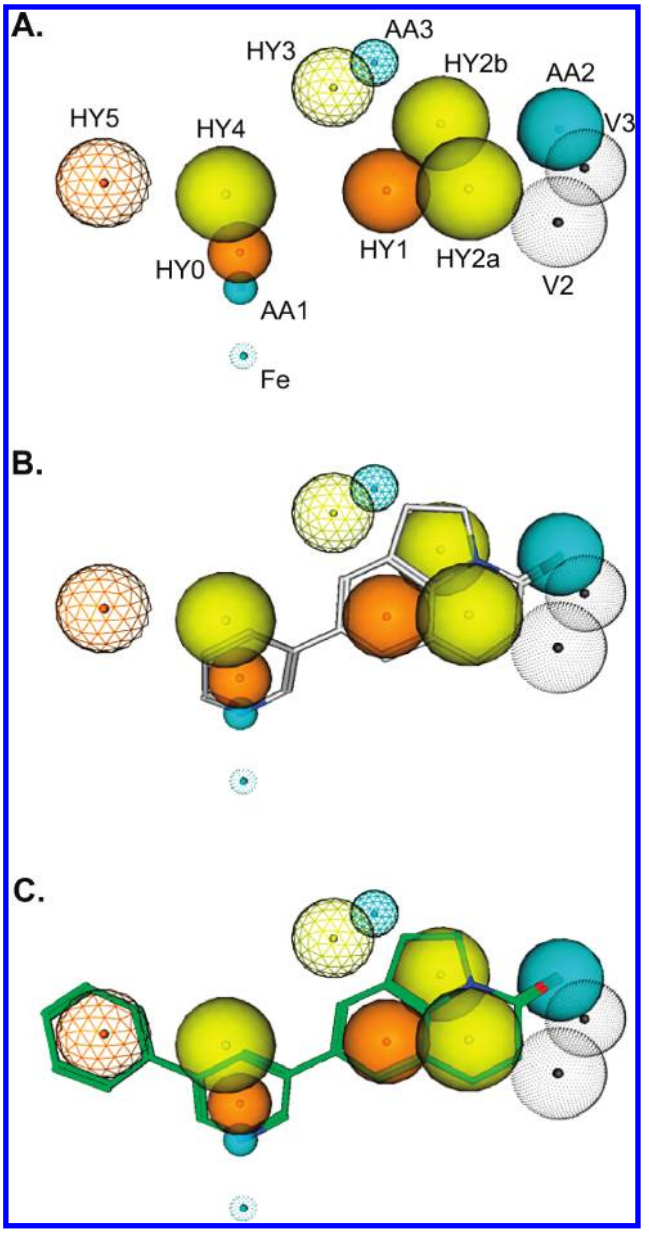

Figure 1. Representation of most important features of the novel pharmacophore model (A). Solid spheres represent essential features for the inhibitory potency, whereas dashed spheres stand for optional features. The pharmacophoric features are colorcoded: cyan, acceptor (AA1−AA3); orange, aromatic (HY0, HY1, HY5); yellow, aromatic/hydrophobic (HY2a/b, HY3b, HY4). In (B) and (C), compounds **4** (white) and **18** (green) are mapped to the pharmacophore model.

of nonsteroidal aldosterone synthase inhibitors with a broad range of activity.

Two pharmacophore models based on inhibitors developed in our group or identified by compound screening have already been described and their predictive capacity has been demonstrated.[20,23] Within the present study, structural information of the CYP11B2 substrates as well as of fadrozole and chemically diverse molecules found in recent patents from Novartis[33] were additionally taken into consideration. The novel pharmacophore model (Figure 1A and Supporting Information Figures S1 and S2) presents several features consistent with our previously described models but also includes two novel

hydrophobic/aromatic features HY4 and HY5. In particular, the essential aromatic (HY0, HY1) and acceptor atom features AA1 (responsible for binding to the heme-iron) and AA2 (forming a hydrogen bond to Glu383), which together define the binding geometry, as well as HY2a and HY2b, were maintained. Features like HY3 and AA3 (Figure 1; rendered as dashed spheres) were included in the design of the new pharmacophore model and for the alignment of the extended inhibitor data set but were not taken into consideration in the rational design efforts herein because they have previously been identified to be optional, leading to no increase of potency. For example, benzylnaphthalene-based inhibitor **33**[20] (Chart 4) that exploits both HY3 and AA3 has he same CYP11B2 potency (IC_{50} = 11 nM) as the unsubstituted counterpart **34**[19] (Chart 4, IC_{50} = 6.2 nM). At the same time, however, **33** shows adverse off-target effects such as CYP2C9 and aromatase inhibition. Nevertheless, these features are representative for the size of the active site of CYP11B2 and could be targeted choosing core structures different from our bicyclic scaffold.

RESULTS AND DISCUSSION

Preliminary studies aiming at the design of nonsteroidal aldosterone synthase inhibitors performed in our laboratory have demonstrated that 3-pyridine substituted naphthalenes provide an ideal molecular scaffold for a strong inhibition of the target enzyme CYP11B2 as well as high selectivity against several other CYP enzymes (e.g., CYP11B1, CYP17, CYP19).[19,21] Most of these molecules, however, revealed two major pharmacological drawbacks: a strong inhibition of the drug metabolizing enzyme CYP1A2 and no inhibitory effect on the aldosterone production in vivo in a rat model. In a recent study, we were able to show that changing the naphthalene by a 3,4-dihydro-1*H*-quinolin-2-one scaffold affords highly potent CYP11B2 inhibitors such as **1**−**3** (Chart 3) with pronounced selectivity against other CYP enzymes including CYP1A2 as well as aldosterone-lowering effects in vivo.[33,34] Among the latter compounds, ethyl-substituted derivative **3** displayed a rather low inhibition of CYP1A2 (IC_{50} = 3.48 μM), thus being a suitable starting point for further optimization.

Herein, we followed a combined ligand- and structure-based approach for the optimization of **3** to identify new, structurally unique molecules, to potentially improve the in vitro and in vivo potency, and to validate our molecular modeling tools. A homology model of CYP11B2 was used in a first design step to rationalize the activity differences of existing compounds, to guide the design of improved inhibitors, and in a later stage to add steric information (excluded volumes) to our pharmacophore hypothesis. One important observation was made by comparing activity and binding mode of a series of *N*-alkyl substituted inhibitors such as **2** and **3**: while the insertion of a methyl group increased the potency (**2**, IC_{50} = 2.6 nM) compared to its unsubstituted derivative **1** (IC_{50} = 28 nM), increasing the size of R reduced the inhibition again (**3**, IC_{50} = 22 nM) or led to a complete loss of activity, respectively (e.g., R = isopropyl, phenyl IC_{50} > 500 nM).[33,35] Docking studies performed for compounds **1**−**3** using FlexX suggested that the decrease of inhibitory action with increasing size of the *N*-alkyl substituents can be explained by a steric clash with amino acids within β-strand 4-1, e.g. Leu382 (Figure 2). In addition, the quinolinone-based inhibitors were found to bind in a consistent geometry defined by two key interactions with the enzyme: (1) a strong coordinative bond to the heme iron and (2) hydrogen bond formation to the backbone-amide of Glu383. Sterically demanding residues at the quinolinone-nitrogen hinder this hydrogen bond formation, whereas small or rigidified substituents may be tolerated. We envisaged that minimizing the steric clash between the ethyl group of **3** and the β4-1 strand of CYP11B2 might increase the inhibitory potency. Eventually, these considerations led to the design of molecules **4** and **5** (Chart 3), in which the ethyl group is incorporated into a 5- or 6-membered ring and thereby the assumed active conformation of the parent molecule is locked.

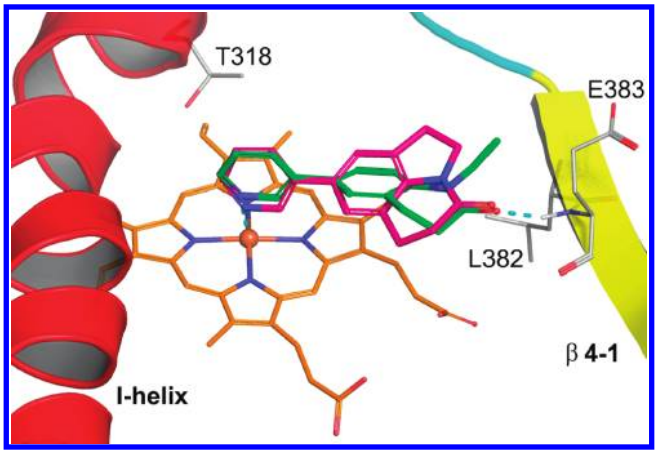

Figure 2. Structure of the CYP11B2−inhibitor complexes of **3** (green) and **4** (magenta). The I-helix (red) and β-sheet β4-1, both lining the active site are rendered as cartoons, whereas the heme is shown in orange sticks with the central iron depicted as ball. Crucial residues for the interaction (Glu383) and for the catalytic activity (Thr318) are also rendered as gray sticks.

Chart 4. Benzyl-Substituted Inhibitor 33 and Unsubstituted Analogue 34

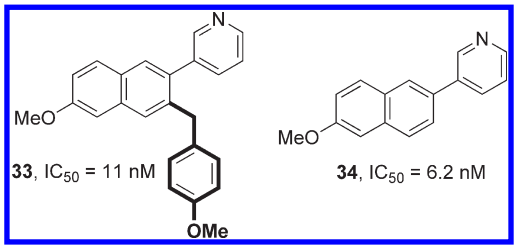

The inhibitory activities of the compounds were determined as described previously using V79 MZh cells expressing either human CYP11B2 or CYP11B1 (Table 1).[10,36] The V79 MZh cells were incubated with [^{14}C]-deoxycorticosterone as substrate and the inhibitor in different concentrations. The product formation was monitored by HPTLC using a phosphoimager. Fadrozole, an aromatase (CYP19) inhibitor with proven ability to reduce corticoid formation in vitro[37] and in vivo,[38] was used as a reference (CYP11B2, IC_{50} = 1 nM; CYP11B1, IC_{50} = 10 nM). Both pyrroloquinolinone **4** and pyrido-condensed analogue **5** were found to be highly potent CYP11B2 inhibitors showing IC_{50} values 10- to 20-fold lower (1.1 or 2.4 nM) compared to the parent molecule **3** (22 nM), indicating that the steric clash with the hydrogen-bond β-strand is minimized. In addition, the selectivity ratios against CYP11B1 are significantly higher (650 and 957) than in the case of **3** (235). Because other CYPs constitute critical off-targets for CYP11B2 inhibitors too, a CYP

Table 1. Inhibition of Human Adrenal CYP11B2 and CYP11B1 in Vitro

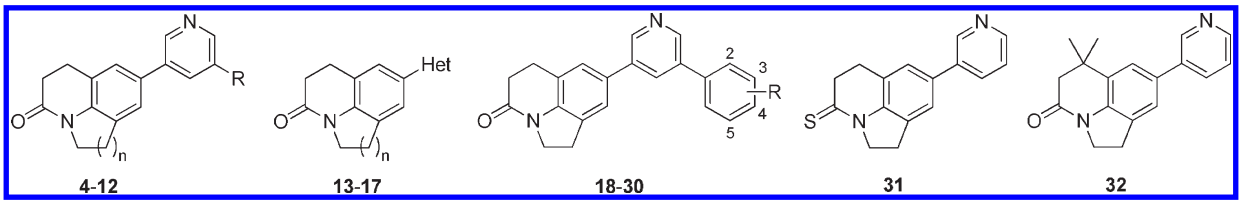

					IC$_{50}$ value[b] (nM)		
compd	*n*	R	Het	% inhibition[a] V79 11B2[c] hCYP11B2	V79 11B2[c] hCYP11B2	V79 11B1[d] hCYP11B1	selectivity factor[e]
4	1	H		90	1.1	715	650
5	2	H		95	2.4	2296	957
6	1	OMe		98	0.6	247	412
7	2	OMe		95	0.9	545	606
8	1	OEt		92	1.0	158	158
9	1	O*i*Pr		96	2.2	103	47
10	1	OH		94	4.3	2045	476
11	1	F		97	4.4	1288	293
12	1	CF_3		96	5.9	141	24
13	1		4-isoquinoline	98	0.2	13	65
14	2		4-isoquinoline	95	0.2	34	170
15	1		4-pyridine	7	nd	nd	nd
16	1		5-pyrimidine	81	56	28546	510
17	1		1-imidazole	87	89	2077	23
18		H		97	1.3	58	45
19		2-F		92	0.7	43	61
20		3-F		97	1.4	490	350
21		4-F		96	0.9	40	44
22		2,5-F		80	3.6	183	51
23		3,4-F		89	2.3	496	215
24		3,5-F		81	18	1748	97
25		2-OMe		86	2.4	128	53
26		3-OMe		86	4.6	1374	299
27		4-OMe		95	1.4	21	15
28		3-OH		92	1.2	44	37
29		3-OCF_3		92	16	2058	129
30		3-CF_3		80	33	4646	141
31				96	1.2	333	278
32				48	nd	nd	nd
fadrozole					1.0	10	10

[a] Mean value of at least three experiments, standard deviation usually less than 10%; inhibitor concentration, 500 nM. [b] Mean value of at least three experiments, standard deviation usually less than 25%, nd = not determined. [c] Hamster fibroblasts expressing human CYP11B2; substrate deoxycorticosterone, 100 nM. [d] Hamster fibroblasts expressing human CYP11B1; substrate deoxycorticosterone, 100 nM. [e] IC$_{50}$ CYP11B1/IC$_{50}$ CYP11B2, nd = not determined.

counterscreen against the steroidogenic enzymes CYP17 and CYP19 (Table 2) as well as the most important hepatic CYP enzymes CYP1A2, CYP2B6, CYP2C9, CYP2C19, CYP2D6, and CYP3A4 (Table 3) was performed to determine the selectivity profiles of **4** and **5**. While the pyrroloquinolinone **4** exhibits a pronounced selectivity against all tested CYPs, compound **5** shows a moderate aromatase (69% inhibition at 0.5 μM) and CYP1A2 inhibition (41% inhibition at 1 μM). Thus, the tricyclic scaffolds of **4** and **5** are promising lead structures for structural optimization, with **4** showing superior overall selectivity.

Most of the molecules derived from compounds **4** and **5** (Table 1) are highly potent aldosterone synthase inhibitors with IC$_{50}$ values in the low nanomolar range (<5 nM). In particular, the isoquinoline derivatives **13** and **14** are the most potent

dx.doi.org/10.1021/jm101470k |*J. Med. Chem.* 2011, 54, 2307–2319

representatives of this series showing subnanomolar IC_{50} values (0.2 nM). However, replacing 3-pyridine by other nitrogen containing heterocycles induces a decrease in inhibitory potency. The 5-pyrimidine (**16**) and 1-imidazole (**17**) derivatives are less active (IC_{50} = 56−89 nM) than the 3-pyridine analogue **4** (IC_{50} = 1.1 nM), and the 4-pyridine compound **15** shows no inhibition of CYP11B2 at a concentration of 500 nM, indicating that the 3-pyridine motif is crucial for the geometry of the two key pharmacophoric features mentioned above and thus for high potency. The same trend was observed previously for the binding properties of a series of substituted pyridylnaphthalenes and 3,4-dihydro-1*H*-quinolin-2-ones.[19,33] The *gem*-dimethyl group in the quinolinone moiety in compound **32** is not tolerated in terms of CYP11B2 potency, while the thioanalogue of **4**, compound **31**, is less selective against CYP11B1 than the parent molecule. In the present study, the chemical modification is mainly directed to the heterocyclic moiety because both potency and selectivity have been identified in previous investigations to be highly dependent on the substitution pattern of the heterocycle.[39] The introduction of small substituents in molecules **6**−**12** does not influence the inhibitory potency (IC_{50} values in the range of 1.0−5.9 nM) but decreases the selectivity against CYP11B1 compared to **4** or **5**. In addition, compounds **5**−**7** show moderate inhibition of some hepatic CYP enzymes (Table 3), while CYP17 and CYP19 are not affected (Table 2). Isoquinoline derivative **14** is a strong inhibitor of hepatic CYP2C9 and CYP2C19.

Table 2. Inhibition of Human CYP17 and CYP19 in Vitro

	% inhibition[a]			% inhibition[a]	
compd	CYP17[b]	CYP19[c]	compd	CYP17[b]	CYP19[c]
4	6	18	**14**	5	<5
5	6	69	**16**	5	5
6	<5	5	**20**	7	6
7	<5	5	**23**	<5	<5
11	<5	<5	**26**	<5	<5
13	6	<5	**31**	11	5

[a] Mean value of three experiments, standard deviation less than 10%. [b] *E. coli* expressing human CYP17; substrate progesterone, 25 μM; inhibitor concentration, 2.0 μM; ketoconazole, IC_{50} = 2.78 μM. [c] Human placental CYP19; substrate androstenedione, 500 nM; inhibitor concentration, 500 nM; fadrozole, IC_{50} = 30 nM.

The pharmacokinetic profile of selected compounds was determined after peroral application to male Wistar rats. Plasma samples were collected over 24 h, and the concentrations were determined by HPLC-MS/MS. Compounds **4**, **6**, and **7** were investigated in a cassette dosing approach (peroral dose = 5 mg/kg) and compared to fadrozole (Figure 3, Table 4). All three compounds show similar terminal half-lifes ($t_{1/2\ z}$ = 2.0−2.9 h), which are in the range of the reference compound fadrozole ($t_{1/2\ z}$ = 3.2 h). However, the absorbance of compounds **4** and **6** (t_{max} = 4 h) occurs slower as the absorbance of fadrozole (t_{max} = 1 h). Within this series, fadrozole shows the highest maximal concentration (C_{max}) in plasma (471 ng/mL) followed by compound **4** (317 ng/mL). The maximal amount of the other test items

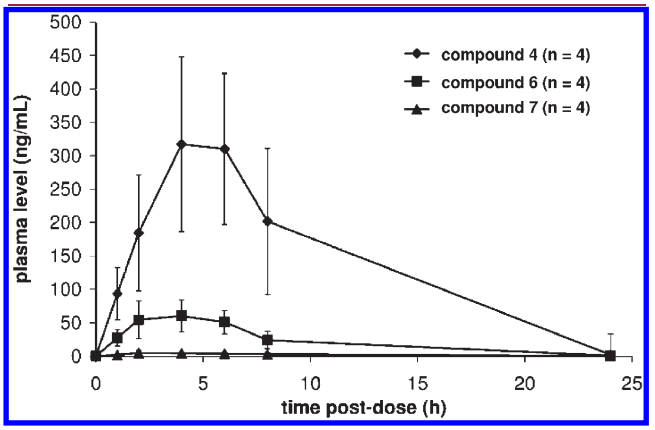

Figure 3. Mean profile (±) SEM of plasma levels (ng/mL) in rat vs time after oral application (5 mg/kg) of compounds **4**, **6**, and **7** determined in a cassette dosing experiment.

Table 4. Pharmacokinetic Profiles of Compounds 4, 6, and 7[a]

compd	$t_{1/2\ z}$ (h)[b]	t_{max} (h)[c]	C_{max} (ng/mL)[d]	$AUC_{0-\infty}$ (ng·h/mL)[e]
4	2.4	4	317	3464
6	2.9	4	60	557
7	2.0	2	4.9	51
fadrozole[f]	3.2	1	471	3207

[a] All compounds were applied perorally (5 mg/kg) to male Wistar rats in a cassette dosing approach. [b] Terminal half-life. [c] Time of maximal concentration. [d] Maximal concentration. [e] Area under the curve. [f] Mean value of two experiments.

Table 3. Inhibition of Selected Hepatic CYP Enzymes in Vitro

	% inhibition[a]											
	CYP1A2[b,c]		CYP2B6[b,d]		CYP2C9[b,e]		CYP2C19[b,f]		CYP2D6[b,g]		CYP3A4[b,h]	
compd	10 μM	1 μM	10 μM	1 μM	10 μM	1 μM	10 μM	1 μM	10 μM	1 μM	10 μM	1 μM
4	43	8	<5	<5	41	6	<5	<5	<5	<5	<5	<5
5	83	41	36	27	40	19	44	8	nd	nd	21	6
6	72	37	8	<5	42	23	30	7	13	9	19	14
7	87	47	nd	nd	63	34	61	11	nd	nd	24	12
14	63	24	nd	nd	97	73	96	67	nd	nd	<5	<5
20	38	9	13	<5	79	39	21	nd	9	<5	43	37

[a] Mean value of two experiments, standard deviation less than 5%. [b] Recombinantly expressed enzymes from baculovirus-infected insect microsomes (Supersomes). [c] Furafylline, IC_{50} = 2.42 μM. [d] Tranylcypromine, IC_{50} = 6.24 μM. [e] Sulfaphenazole, IC_{50} = 318 nM. [f] Tranylcypromine, IC_{50} = 5.95 μM. [g] Quinidine, IC_{50} = 14 nM. [h] Ketoconazole, IC_{50} = 57 nM.

dx.doi.org/10.1021/jm101470k |*J. Med. Chem.* 2011, 54, 2307–2319

(**6** and **7**) found in the plasma after peroral application is significantly lower (<50 ng/mL). Using the area under the curve ($AUC_{0-\infty}$) as a ranking criterion, pyrroloquinolinone **4** exhibits the highest bioavailability (3464 ng·h/mL), which is in the range of the $AUC_{0-\infty}$ of fadrozole (3207 ng·h/mL). Methoxylation of the heterocycle as accomplished in **6** results in a significant decrease of the $AUC_{0-\infty}$ (557 ng·h/mL). A further decrease is observed for the corresponding pyridoquinolinone **7** (51 ng·h/mL). This may be due to, for example, either excessive metabolism (due to the electron donating ability of the methoxy substituent and, therefore, higher sensitivity to oxidative metabolism) or to reduced absorption.

The further optimization process, eventually leading to compounds **18**−**30**, was assisted by our pharmacophore model. Compound **4** already shows a reasonable fit to the pharmacophore hypothesis by exploiting the key pharmacophoric features AA1, AA2, HY0, and HY1, together with overlapping HY2a and HY2b (Figure 1B). In the new pharmacophore model, two additional hydrophobic/aromatic areas were identified adjacent to the pyridine ring, HY4 and HY5, which is located in the putative *meta*-(5)-position. Rationalizing the given information, we envisaged that compound **18**, whose additional benzene moiety perfectly overlaps with the aromatic moiety HY5 (Figure 1C), is a promising starting point for developing new inhibitors. Indeed, benzene substituted analogue **18** was found to be a potent inhibitor of CYP11B2 although no increase of potency compared to the parent molecule **4** was observed. The same trend was observed for the other molecules of the series, thereby rendering the ligands less efficient. Thus, HY5 represents an optional pharmacophoric feature (like HY3 and AA3) and is associated with a decreased selectivity against CYP11B1. The CYP17, CYP19, and hepatic CYP activity of selected molecules was found to be low or moderate. Compound **20** displays a distinct inhibition of CYP2C9 (79% at a concentration of 10 μM) but is rather selective against other CYP enzymes (IC_{50} > 10 μM). However, as presented in Table 3, none of the substituted derivatives is as selective as the unsubstituted parent compound **4**.

Given the rather constant IC_{50} values of CYP11B2 inhibition of the molecules presented herein (the majority of the compounds shows inhibition in the range of 1−5 nM), structure−activity relationships with respect to the inhibition of 11β-hydroxylase (CYP11B1) and thus selectivity become particularly interesting. On the one hand, selectivity is influenced by the ring-size of the carbocycle condensed to the quinolinone moiety (HY4). Within the series of pyrido-condensed compounds (**5**, **7**, and **14**), the CYP11B1 inhibition is significantly decreased compared to the corresponding pyrroloquinolinone analogues (**4**, **6**, and **13**), whereas the CYP11B2 inhibition is in a comparable range. This leads to an enhanced selectivity for the pyridoquinolinone derivatives. Pyridoquinolinone **5** is the most selective compound of the present series (selectivity factor = 957) and is 100-fold more selective than fadrozole (selectivity factor = 10). This experimental result is particularly noteworthy with respect to the high homology of the two CYP11B isoforms. On the other hand, the substitution pattern of the pyridine moiety was found to significantly influence the CYP11B1 selectivity. The size of substituents in 5-position (HY5) of the heterocycle plays a crucial role for the CYP11B1 inhibition. This becomes particularly evident in the series of pyrroloquinolinone compounds with alkoxy-substituted heterocycle. The inhibitory potency at CYP11B1 increases with the substituent size in the order **4** (R = H, IC_{50} = 715 nM) < **6** (R = OMe, IC_{50} = 247 nM) < **8** (R = OEt, IC_{50} = 158 nM) < **9** (R = O*i*Pr, IC_{50} = 103 nM). At the same time, the inhibition of CYP11B2 is in a comparable range for all compounds (IC_{50} = 0.6−2.2 nM) with the consequence that the selectivity factor decreases in the same order from 650 (**4**) to 47 (**9**). A pronounced increase in CYP11B1 inhibition is observed in the case of the introduction of additional aryl moieties. Replacing 3-pyridine by 4-isoquinoline results in a dramatic increase in CYP11B1 potency for both the pyrrolo-condensed (**13**, increase by a factor of 55) and pyrido-condensed (**14**, factor 68) derivative, whereas the CYP11B2 inhibition increases to a minor degree (factor 6−12). The same trend can be observed for several compounds with additional aryl substituent in 5-position of the pyridine moiety (e.g., **18**, **19**, **31**, **25**, **27**, and **28**). The latter compounds display a CYP11B2 inhibition in a range of 0.7−2.4 nM, which is comparable to the unsubstituted parent compound **4** (IC_{50} = 1.1 nM). However, the CYP11B1 inhibition increases up to 36-fold compared to **4** (IC_{50} = 715 nM) to IC_{50} values of 21−128 nM, corresponding to a rather low selectivity (factor 15−61). Apparently, the introduction of additional aromatic rings and to a minor degree also sterically demanding aliphatic residues (e.g., isopropoxy) in the pyridine moiety leads to additional interactions of the inhibitors with CYP11B1. Moreover, it is striking that *meta* substituents in the aryl moiety can trigger CYP11B1 selectivity again. With exception of the 3-hydroxy derivative **28**, all compounds bearing a substituent in 3-position of the benzene moiety (i.e., **20**, **23**, **24**, **26**, **29**, and **30**) exhibit a decreased CYP11B1 potency with IC_{50} values in a range of 490−4646 nM and thus selectivity factors of up to 350 (**20**). This off/on-switch of CYP11B1 potency is of particular interest. From unsubstituted parent compound **4** (IC_{50} = 715 nM), derivatization with phenyl in the 5-position of the pyridine moiety leads to a significant increase of inhibitory potency in compound **18** (IC_{50} = 58 nM), whereas the *meta*-fluorophenyl analogue **20** exhibits a low inhibitory potency again (IC_{50} = 490 nM). At the same time, these three compounds display the same aldosterone synthase activity (IC_{50} = 1.1−1.4 nM). This means that a variety of sterically demanding substituents in the pyridine moiety is readily tolerated in the CYP11B2 binding pocket, however, lead to no further stabilization of the complexes formed by coordination of the heme iron by the heterocyclic nitrogen. On the other hand, 3-pyridine substituted pyrroloquinolinone derivatives such as **4** are per se rather poor CYP11B1 inhibitors and require an additional benzene moiety and thus a further stabilization of the formed complexes for basal inhibitory potency. Among these compounds, there are highly potent CYP11B1 inhibitors, for example, isoquinoline derivative **13** (IC_{50} = 13 nM) and *para*-methoxyphenyl derivative **27** (IC_{50} = 21 nM). Obviously the *meta*-substituted analogues do not adequately fit into the CYP11B1 binding pocket or loose contact to the heme iron while minimizing unfavorable contacts with the enzyme.

CONCLUSION

Herein, we have presented the rational design of a series of pyrroloquinolinone-based inhibitors of CYP11B2, a promising target for the treatment of aldosterone-mediated disorders such as hypertension and congestive heart failure. The variation of the substitution pattern was guided by a pharmacophore hypothesis based on data from structurally diverse aldosterone synthase inhibitors and validated by docking studies using a newly developed homology model.

The present study provides extensive SAR results relating to CYP11B2 and CYP11B1 inhibition. The influence of certain structural modifications on the 11β-hydroxylase (CYP11B1) activity is particularly noteworthy. On the one hand, CYP11B1 inhibition is an important selectivity criterion for aldosterone synthase inhibitors. On the other hand, selective CYP11B1 inhibitors could be used for the treatment of Cushing's syndrome and metabolic syndrome. Although several potent CYP11B1 inhibitors have been described previously,[40] in-depth SAR studies usually focused on the CYP11B2 activity. Herein, we clearly identified structural features important for high inhibitory CYP11B1 potency such as sterically demanding lipophilic or aromatic residues in the heterocyclic moiety or condensed to the heterocycle, leading to a series of highly potent yet unselective 11β-hydroxylase inhibitors (e.g., *para*-methoxyphenyl derivative **27**, IC_{50} = 21 nM). Subtle structural modifications of these compounds, such as introduction of *meta*-substituents into the phenyl moiety, led to a significant loss of CYP11B1 inhibition again, providing selective CYP11B2 inhibitors.

Finally, pyrroloquinolinone **4** emerged from the present study as a keenly optimized lead molecule. Beside strong aldosterone synthase inhibiting properties, this inhibitor is orally available in the range of the marketed drug fadrozole and shows no off-target effects against similar enzymes (e.g., steroidogenic and hepatic CYPs). Currently, further studies with inhibitor **4** are underway to evaluate aldosterone-lowering effects in vivo as well as beneficial effects in appropriate disease models.

EXPERIMENTAL SECTION

Chemical and Analytical Methods. Melting points were measured on a Mettler FP1 melting point apparatus and are uncorrected. ^{1}H NMR and ^{13}C spectra were recorded on a Bruker DRX-500 instrument. Chemical shifts are given in parts per million (ppm), and tetramethylsilane (TMS) was used as internal standard for spectra obtained in DMSO-d_6 and $CDCl_3$. All coupling constants (J) are given in hertz. Reagents were used as obtained from commercial suppliers without further purification. Solvents were distilled before use. Dry solvents were obtained by distillation from appropriate drying reagents and stored over molecular sieves. Flash chromatography was performed on silica gel 40 (35/40−63/70 μM) with petroleum ether/ethyl acetate mixtures as eluents, and the reaction progress was determined by thin-layer chromatography analyses on Alugram SIL G/UV254 (Macherey Nagel). Visualization was accomplished with UV light and $KMnO_4$ solution. All microwave irradiation experiments were carried out in a CEM-Discover monomode microwave apparatus.

The purity of the compounds was determined by LC/MS and/or elemental analysis and was ≥95%. The Surveyor-LC system consisted of a pump, an autosampler, and a PDA detector. Mass spectrometry was performed on a TSQ Quantum (Thermo Electron Corporation, Dreieich, Germany). The triple quadrupole mass spectrometer was equipped with an electrospray interface (ESI). In some cases, ionization was accomplished by APCI. The system was operated by the standard software Xcalibur. A RP18 100-3 column (Macherey-Nagel GmbH, Duehren, Germany) was used as stationary phase. All solvents were HPLC grade. The HPLC method used for the purity determination started with a 20 min gradient from 100% water containing 1 ‰ TFA to 100% methanol/acetonitrile (4/1) containing 1 ‰ TFA. The injection volume was 1−10 μL, and flow rate was set to 350 μL/min. MS analysis was carried out at a spray voltage of 3800 V, a capillary temperature of 350 °C, and a source CID of 10 V. Spectra were acquired in positive ionization mode from 100 to 1000 m/z and full scan UV-mode.

The following compounds were prepared according to previously described procedures: 1,2,5,6-tetrahydro-4*H*-pyrrolo[3,2,1-*ij*]quinolin-4-one (**4b**),[24] 2,3,6,7-tetrahydro-1*H*,5*H*-pyrido[3,2,1-*ij*]quinolin-5-one (**5b**),[24] 5-bromopyridin-3-ol (**8b**),[39] 3-bromo-5-ethoxypyridine (**8a**).[39]

Synthesis of the Target Compounds. *Procedure A.* Boronic acid (1 equiv), aryl bromide or (1.3−1.5 equiv), and tetrakis-(triphenylphosphane)palladium(0) (5 mol %) were suspended in toluene/ethanol 4/1 to give a 0.07−0.1 M solution of boronic acid under an atosphere of nitrogen. To this was added a 1 N aqueous solution of Na_2CO_3 (6 equiv). The mixture was then refluxed for 12−18 h, cooled to room temperature, diluted with water, and extracted several times with ethyl acetate. The combined extracts were dried over $MgSO_4$, concentrated, and purified by flash chromatography on silica gel (petroleum ether/ethyl acetate mixtures) and/or crystallization.

Procedure B.[25] Boronic acid (0.75 mmol, 1 equiv), aryl bromide or -triflate (0.9−1.3 equiv), and tetrakis(triphenylphosphane)palladium(0) (43 mg, 37.5 μmol, 5 mol %) were suspended in 1.5 mL of DMF in a 10 mL septum-capped tube containing a stirring magnet. To this was added a solution of $NaHCO_3$ (189 mg, 2.25 mmol, 3 equiv) in 1.5 mL of water, and the vial was sealed with an Teflon cap. The mixture was irradiated with microwaves for 15 min at a temperature of 150 °C with an initial irradiation power of 100 W. After the reaction, the vial was cooled to 40 °C, the crude mixture was partitioned between ethyl acetate and water, and the aqueous layer was extracted three times with ethyl acetate. The combined organic layers were dried over $MgSO_4$, and the solvents were removed in vacuo. The coupling products were obtained after flash chromatography on silica gel (petroleum ether/ethyl acetate mixtures) and/or crystallization.

*8-Pyridin-3-yl-1,2,5,6-tetrahydro-4H-pyrrolo[3,2,1-ij]quinolin-4-one (**4**).* Compound **4** was obtained according to procedure A from **4a** (5.19 g, 20.6 mmol) and 3-pyridineboronic acid (2.30 g, 18.7 mmol) after flash chromatography on silica gel (ethyl acetate, R_f = 0.08) and crystallization from acetone/diethylether as colorless plates (2.29 g, 9.16 mmol, 49%), mp 153−154 °C. ^{1}H NMR (500 MHz, $CDCl_3$): δ 2.72 (t, ^3J = 7.8 Hz, 2H), 3.03 (t, ^3J = 7.8 Hz, 2H), 3.25 (t, ^3J = 8.5 Hz, 2H), 4.13 (t, ^3J = 8.5 Hz, 2H), 7.20 (s, 1H), 7.28 (s, 1H), 7.32 (ddd, ^3J = 7.8 Hz, ^3J = 4.8 Hz, ^5J = 0.5 Hz, 1H), 7.79 (ddd, ^3J = 7.8 Hz, ^4J = 2.2 Hz, ^4J = 1.6 Hz, 1H), 8.54 (dd, ^3J = 4.7 Hz, ^4J = 1.4 Hz, 1H), 8.59 (d, ^4J = 2.0 Hz, 1H). ^{13}C NMR (125 MHz, $CDCl_3$): δ 24.5, 27.7, 31.6, 45.5, 120.7, 122.4, 123.5, 124.7, 129.9, 133.5, 134.0, 136.7, 141.6, 148.1, 167.6. MS m/z 251.09 (MH^+). Purity by LC/MS: 100% (R_t = 7.00 min). Anal. calcd for ($C_{16}H_{14}N_2O$) C 76.78, H 5.64, N 11.19; found C 77.13, H 5.52, N 11.25.

*9-Pyridin-3-yl-1,2,6,7-tetrahydro-5H-pyrido[3,2,1-ij]quinolin-3-one (**5**).* Compound **5** was obtained according to procedure B from **5a** (266 mg, 1.0 mmol) and 3-pyridineboronic acid (92 mg, 0.75 mmol) after flash chromatography on silica gel (petroleum ether/ethyl acetate, 2/3, R_f = 0.12) and crystallization from acetone/diethylether as colorless needles (116 mg, 0.44 mmol, 59%), mp 122−123 °C. ^{1}H NMR (500 MHz, $CDCl_3$): δ 1.97 (m, 2H), 2.69 (t, ^3J = 7.2 Hz, 2H), 2.86 (t, ^3J = 6.3 Hz, 2H), 2.95 (t, ^3J = 7.2 Hz, 2H), 3.90 (t, ^3J = 6.1 Hz, 2H), 7.20−7.24 (m, 2H), 7.33 (ddd, ^3J = 7.9 Hz, ^3J = 4.7 Hz, ^5J = 0.6 Hz, 1H), 7.81 (ddd, ^3J = 7.9 Hz, ^4J = 2.3 Hz, ^4J = 1.5 Hz, 1H), 8.55 (dd, ^3J = 4.8 Hz, ^4J = 1.5 Hz, 1H), 8.80 (m, 1H). ^{13}C NMR (125 MHz, $CDCl_3$): δ 21.4, 25.4, 27.4, 31.4, 41.0, 123.5, 124.4, 125.9, 126.2, 126.4, 131.9, 133.8, 135.9, 136.2, 148.0, 148.2, 169.4. MS m/z 264.96 (MH^+). Purity by LC/MS: 99.61% (R_t = 7.93 min).

*8-Isoquinolin-4-yl-1,2,5,6-tetrahydro-4H-pyrrolo[3,2,1-ij]quinolin-4-one (**13**).* Compound **13** was obtained according to procedure B from **4a** (252 mg, 1.0 mmol) and 4-isoquinolineboronic acid (227 mg, 0.9 mmol) after flash chromatography on silica gel (petroleum ether/ethyl acetate, 2/3, R_f = 0.13) as colorless needles (93 mg, 0.31 mmol, 34%), mp 184−185 °C. ^{1}H NMR (500 MHz, $CDCl_3$): δ 2.75 (t, ^3J = 7.8 Hz, 2H), 3.05 (t, ^3J = 7.8 Hz, 2H), 3.28 (t, ^3J = 8.4 Hz, 2H), 4.16 (t, ^3J = 8.4 Hz, 2H), 7.13 (s, 1H), 7.20 (s, 1H), 7.62 (m, 1H), 7.67 (m, 1H), 7.91 (d, ^3J = 8.5 Hz, 1H), 8.02 (d, ^3J = 7.9 Hz, 1H), 8.44 (s, 1H), 9.22 (s, 1H).

^{13}C NMR (125 MHz, $CDCl_3$): δ 24.4, 27.8, 31.6, 45.4, 120.2, 124.7, 125.1, 127.1, 127.4, 127.9, 128.4, 129.3, 130.5, 132.2, 133.2, 134.2, 141.3, 142.8, 151.8, 167.6. MS m/z 300.95 (MH^+). Purity by LC/MS: 100% (R_t = 8.72 min).

*8-(5-Phenylpyridin-3-yl)-1,2,5,6-tetrahydro-4H-pyrrolo[3,2,1-ij]-quinolin-4-one (**18**).* Compound **18** was obtained according to procedure A from **6a** (325 mg, 1.07 mmol) and 3-bromo-5-phenylpyridine (301 mg, 1.28 mmol) after flash chromatography on silica gel (petroleum ether/ethyl acetate, 2/3, R_f = 0.09) as colorless plates (150 mg, 0.46 mmol, 43%), mp 188−189 °C. ^{1}H NMR (500 MHz, $CDCl_3$): δ 2.73 (t, ^3J = 7.7 Hz, 2H), 3.05 (t, ^3J = 7.9 Hz, 2H), 3.26 (t, ^3J = 8.5 Hz, 2H), 4.14 (t, ^3J = 8.5 Hz, 2H), 7.26 (s, 1H), 7.34 (s, 1H), 7.42 (m, 1H), 7.49 (m, 2H), 7.63 (dd, ^3J = 6.9 Hz, ^4J = 1.6 Hz, 2H), 7.98 (m, 1H), 8.75 (d, ^4J = 1.9 Hz, 1H), 8.78 (d, ^4J = 1.9 Hz, 1H). ^{13}C NMR (125 MHz, $CDCl_3$): δ 24.5, 27.8, 31.6, 45.5, 120.7, 122.4, 124.8, 127.2, 128.3, 129.1, 129.9, 132.7, 133.3, 136.7, 136.8, 137.7, 141.7, 146.5, 146.6, 167.5. MS m/z 327.07 (MH^+). Purity by LC/MS: 99.60% (R_t = 13.74 min).

*8-[5-(3-Fluorophenyl)-pyridin-3-yl]-1,2,5,6-tetrahydro-4H-pyrrolo-[3,2,1-ij]quinolin-4-one (**20**).* Compound **20** was obtained according to procedure A from **6a** (360 mg, 1.20 mmol) and **20a** (378 mg, 1.50 mmol) after flash chromatography on silica gel (petroleum ether/ethyl acetate, 2/3, R_f = 0.08) as colorless needles (97 mg, 0.28 mmol, 23%), mp 181−182 °C. ^{1}H NMR (500 MHz, $CDCl_3$): δ 2.73 (t, ^3J = 7.9 Hz, 2H), 3.05 (t, ^3J = 7.9 Hz, 2H), 3.27 (t, ^3J = 8.5 Hz, 2H), 4.14 (t, ^3J = 8.5 Hz, 2H), 7.12 (m, 1H), 7.26 (s, 1H), 7.31−7.35 (m, 2H), 7.40−7.48 (m, 2H), 7.96 (m, 1H), 8.76 (d, ^4J = 2.0 Hz, 1H), 8.77 (d, ^4J = 2.2 Hz, 1H). ^{13}C NMR (125 MHz, $CDCl_3$): δ 24.5, 27.7, 31.6, 45.5, 120.8, 114.2 (d, $^2J_{C,F}$ = 22.0 Hz), 115.2 (d, $^2J_{C,F}$ = 21.9 Hz), 122.5, 122.9, 124.8, 130.0, 130.7 (d, $^3J_{C,F}$ = 8.3 Hz), 132.7, 133.0, 135.5, 136.9, 139.9 (d, $^3J_{C,F}$ = 7.3 Hz), 141.9, 146.2, 147.0, 163.3 (d, $^1J_{C,F}$ = 247 Hz), 167.5. MS m/z 345.05 (MH^+). Purity by LC/MS: 98.75% (R_t = 11.62 min). Anal. calcd for ($C_{22}H_{17}FN_2O$) C 76.73, H 4.98, N 8.13; found C 76.54, H 5.19, N 8.28.

Biological Methods. (1) Enzyme preparations. The inhibition of CYP17 was investigated using the 50000*g* sediment of the *E. coli* homogenate recombinantly expressing human CYP17 and progesterone (25 μM) as substrate.[41] The inhibition values were measured at an inhibitor concentration of 2 μM. The inhibition of CYP19 at an inhibitor concentration of 500 nM was determined in vitro with human placental microsomes and [1β-^{3}H]androstenedione as substrate as described by Thompson and Siiteri[42] using our modification.[11,36] Inhibition of hepatic CYP enzymes was measured using recombinantly expressed enzymes from baculovirus-infected insect microsomes (Supersomes). (2) Enzyme assays. The following enzyme assays were performed as previously described: CYP17 and CYP19. (3) Activity and selectivity assay using V79 cells. V79 MZh 11B1 and V79 MZh 11B2 cells[10,36] were incubated with [4-^{14}C]-11-deoxycorticosterone as substrate and inhibitor in at least three different concentrations. The enzyme reactions were stopped by addition of ethyl acetate. After vigorous shaking and a centrifugation step (10000*g*, 2 min), the steroids were extracted into the organic phase, which was then separated. The conversion of the substrate was analyzed by HPTLC and a phosphoimaging system as described.[10,36] (4) Inhibition of human hepatic CYP enzymes. The recombinantly expressed enzymes from baculovirus-infected insect microsomes (Supersomes) were used and the manufacturer's instructions (www.gentest.com) were followed. (5) In vivo pharmacokinetics. Animal trials were conducted in accordance with institutional and international ethical guidelines for the use of laboratory animals. Male Wistar rats weighing 260−280 g (Janvier, France) were housed in a temperature-controlled room (20−24 °C) and maintained in a 12 h light/12 h dark cycle. Food and water were available ad libitum. The animals were anaesthetised with a ketamine (90 mg/kg)/xylazine (10 mg/kg) mixture and cannulated with silicone tubing via the right jugular vein. Prior to the first blood sampling, animals were connected to a counterbalanced system and tubing to perform blood sampling in the freely moving rat. Separate stock solutions (5 mg/mL) were prepared for the tested compounds in labrasol/water (1:1; v/v), leading to a clear solution. Immediately before application, the cassette dosing mixture was prepared by adding equal volumes of the stock solutions to end up with a final concentration of 1 mg/mL for each compound. The mixture was applied perorally to four rats with an injection volume of 5 mL/kg (Time 0). Blood samples (250 μL) were collected 1 h before application and 1, 2, 4, 6, 8, and 24 h thereafter. They were centrifuged at 650*g* for 10 min at 4 °C, and then the plasma was harvested and kept at −20 °C until LC/MS analysis. To 50 μL of rat plasma sample and calibration standard, 100 μL of acetonitrile containing the internal standard was added. Samples and standards were vigorously shaken and centrifuged for 10 min at 6000*g* and 20 °C. For the test items, an additional dilution was performed by mixing 50 μL of the particle free supernatant with 50 μL of water. An aliquot was transferred to 200 μL sampler vials and subsequently subjected to LC-MS/MS. HPLC-MS/MS analysis and quantification of the samples was carried out on a Surveyor-HPLC system coupled with a TSQ Quantum (ThermoFinnigan) triple quadrupole mass spectrometer equipped with an electrospray interface (ESI). The mean of absolute plasma concentrations (±SEM) was calculated for the four rats, and the regression was performed on group mean values. The pharmacokinetic analysis was performed using a noncompartment model (PK Solutions 2.0, Summit Research Services).

Computational Methods. (1) Pharmacophore modeling. The ligands of both the training set and the test database were built in MOE,[43] minimized, and conformers then generated using MOE's Conformation Import tool. Structural data of the enzyme, such as heme complexation and conformational hindrances of active site residues, were used to direct the preparation of both ligands and pharmacophore queries. First, we superimposed all high-active compounds of the training set according to the pharmacophore hypothesis of Lucas et al.,[17] and then we set up a preliminary pharmacophore query using the Pharmacophore Consensus application of MOE. This utility calculates a query composed of all features of all molecules, with an indication of the proportion of shared features. The whole training database was now searched by using the preliminary query, and the results of the search were then examined to suggest modifications to the query in order to increase the recognition rate of highly active compounds. Finally, the best results were obtained when the pharmacophore query was not overconstrained, hence when AA1/HY0 and HY1 were marked as essential and a partial match of a minimum of 7 (out of 11) features was permitted. A visual inspection of the output of the search revealed molecules that should be ruled out for steric reasons. An additional volume constraint was therefore added to the query to help further constrain the search. Using the Union feature of the Pharmacophore Query Editor, excluded five volume spheres were positioned coincident with atoms in the active site of the homology model of CYP11B2. (2) Protein modeling and docking. A multitemplate strategy was followed to build a set of homology models of CYP11B2 for which the crystal structures of the human CYP19 (3eqm), 3A4 (1tqn), 1A2 (2hi4), 2E1 (3e6i), 2C9 (1og2), and 2D6 (2f9q) enzymes were used. CYP19, CYP2C9, and CYP3A4 have been trialed out as core template, necessary for a correct alignment of all the different CYPs, with CYP2C9 resulting the most appropriate one. Sequence alignment of CYP19, 3A4, 1A2, 2E1, 2C9, and 2D6 was accomplished by means of T-COFFEE/ESPRESSO[44] and final manual adjustments. The latter was strongly supported by secondary structure predictions by means of Jpred[45] and PSIPRED.[46] The homology models were generated with MODELLER9v7[47] and evaluated by means of Procheck,[48] Prosa2003,[49,50] and DOPE score. Best ranked models were then further validated by docking a series of aldosterone synthase within a large IC_{50} range using FlexX docking software.[51] In this study, selected compounds were docked into the refined homology model using FlexX-pharm. A

directed heme−Fe-N interaction perpendicular to the heme plane was set as constraint to ensure the right binding mode of the inhibitors with the heme cofactor. All the resting ligand−protein interaction parameters and geometries were used as the default. The protein−ligand interactions were analyzed using the LigX module of MOE software.

■ ASSOCIATED CONTENT

Supporting Information. Syntheses and spectroscopic data of the target compounds **6**−**12**, **14**−**17**, **19**, **22**−**32**, full experimental details and spectroscopic characterization of the reaction intermediates **4a**−**6a**, **9a**, **19a**−**30a**, **32a**, **32b**, and pharmacophore geometric properties. This material is available free of charge via the Internet at http://pubs.acs.org.

■ AUTHOR INFORMATION

Corresponding Author

*Phone: +49-681-30270300. Fax: +49-681-30270308. E-mail: rwh@mx.uni-saarland.de. Homepage: http://www.PharmMedChem.de.

Present Addresses

[§]Grünenthal Pharma GmbH, Global Drug Discovery, Zieglerstrasse 6, 52078 Aachen, Germany.

■ ACKNOWLEDGMENT

We thank Gertrud Schmitt and Jeannine Jung for their help in performing the in vitro tests. We would also like to acknowledge the undergraduate research participants Judith Horzel, Helena Rübel, and Michael Zender whose work contributed to the presented results. The investigation of the hepatic CYP profile by Dr. Ursula Müller-Vieira and the pharmacokinetic studies by Dr. Barbara Birk, Pharmacelsus CRO, Saarbrücken, are highly appreciated. S.L. is grateful to Saarland University for a scholarship (Landesgraduierten-Förderung). Thanks are due to Prof. J. J. Rob Hermans, University of Maastricht, The Netherlands, for supplying the V79 CYP11B1 cells, and Prof. Rita Bernhardt, Saarland University, for supplying the V79 CYP11B2 cells.

■ ABBREVIATIONS USED

Ang II, angiotensin II; AUC, area under the curve; BPin, pinacol boronate; CHF, congestive heart failure; CYP, cytochrome P450; CYP11B1, 11β-hydroxylase; CYP11B2, aldosterone synthase; CYP17, 17α-hydroxylase-17,20-lyase; CYP19, aromatase; Het, heteroaryl; MR, mineralocorticoid receptor; NBS, *N*-bromosuccinimide; RAAS, renin-angiotensin-aldosterone system; SAR, structure−activity relationship; HY, hydrophobic or aromatic pharmacophore feature; AA, acceptor atom feature

■ REFERENCES

(1) Weber, K. T. Aldosterone in congestive heart failure. *N. Engl. J. Med.* **2001**, *345*, 1689–1697.

(2) (a) Brilla, C. G. Renin−angiotensin−aldosterone system and myocardial fibrosis. *Cardiovasc. Res.* **2000**, *47*, 1–3. (b) Lijnen, P.; Petrov, V. Induction of cardiac fibrosis by aldosterone. *J. Mol. Cell. Cardiol.* **2000**, *32*, 865–879.

(3) (a) Struthers, A. D. Aldosterone escape during angiotensin-converting enzyme inhibitor therapy in chronic heart failure. *J. Card. Failure* **1996**, *2*, 47–54. (b) Sato, A.; Saruta, T. Aldosterone escape during angiotensin-converting enzyme inhibitor therapy in essential hypertensive patients with left ventricular hypertrophy. *J. Int. Med. Res.* **2001**, *29*, 13–21.

(4) (a) Pitt, B.; Zannad, F.; Remme, W. J.; Cody, R.; Castaigne, A.; Perez, A.; Palensky, J.; Wittes, J. The effect of spironolactone on morbidity and mortality in patients with severe heart failure. *N. Engl. J. Med.* **1999**, *341*, 709–717. (b) Pitt, B.; Remme, W.; Zannad, F.; Neaton, J.; Martinez, F.; Roniker, B.; Bittman, R.; Hurley, S.; Kleiman, J.; Gatlin, M. Eplerenone, a selective aldosterone blocker, in patients with left ventricular dysfunction after myocardial infarction. *N. Engl. J. Med.* **2003**, *348*, 1309–1321.

(5) (a) Hu, X.; Bolten, C. W. Adrenal corticosteroids, their receptors and hypertension. *Drug Dev. Res.* **2006**, *67*, 871–883. (b) Hu, X.; Li, S.; McMahon, E. G.; Lala, D. S.; Rudolph, A. E. Molecular mechanisms of mineralocorticoid receptor antagonism by eplerenone. *Mini. Rev. Med. Chem.* **2005**, *5*, 709–718.

(6) Juurlink, D. N.; Mamdani, M. M.; Lee, D. S.; Kopp, A.; Austin, P. C.; Laupacis, A.; Redelmeier, D. A. Rates of hyperkalemia after publication of the Randomized Aldactone Evaluation Study. *N. Engl. J. Med.* **2004**, *351*, 543–551.

(7) Delcayre, C.; Swynghedauw, B. Molecular mechanisms of myocardial remodeling. The role of aldosterone. *J. Mol. Cell. Cardiol.* **2002**, *34*, 1577–1584.

(8) (a) Wehling, M. Specific, nongenomic actions of steroid hormones. *Annu. Rev. Physiol.* **1997**, *59*, 365–393. (b) Lösel, R.; Wehling, M. Nongenomic actions of steroid hormones. *Nature Rev. Mol. Cell. Biol.* **2003**, *4*, 46–55.

(9) Hartmann, R. W. Selective inhibition of steroidogenic P450 enzymes: current status and future perspectives. *Eur. J. Pharm. Sci.* **1994**, *2*, 15–16.

(10) Ehmer, P. B.; Bureik, M.; Bernhardt, R.; Müller, U.; Hartmann, R. W. Development of a test system for inhibitors of human aldosterone synthase (CYP11B2): Screening in fission yeast and evaluation of selectivity in V79 cells. *J. Steroid Biochem. Mol. Biol.* **2002**, *81*, 173–179.

(11) (a) Hartmann, R. W.; Batzl, C. Aromatase inhibitors. Synthesis and evaluation of mammary tumor inhibiting activity of 3-alkylated 3-(4-aminophenyl)piperidine-2,6-diones. *J. Med. Chem.* **1986**, *29*, 1362–1369. (b) Le Borgne, M.; Marchand, P.; Duflos, M.; Delevoye-Seiller, B.; Piessard-Robert, S.; Le Baut, G.; Hartmann, R. W.; Palzer, M. Synthesis and in vitro evaluation of 3-(1-azolylmethyl)-1*H*-indoles and 3-(1-azolyl-1-phenylmethyl)-1*H*-indoles as inhibitors of P450 arom. *Arch. Pharm. (Weinheim, Germany)* **1997**, *330*, 141–145.

(12) (a) Hille, U. E.; Hu, Q.; Vock, C.; Negri, M.; Bartels, M.; Müller-Vieira, U.; Lauterbach, T.; Hartmann, R. W. Novel CYP17 inhibitors: synthesis, biological evaluation, structure−activity relationships and modelling of methoxy- and hydroxy-substituted methyleneimidazolyl biphenyls. *Eur. J. Med. Chem.* **2009**, *44*, 2765–2775. (b) Hu, Q.; Yin, L.; Jagusch, C.; Hille, U. E.; Hartmann, R. W. Isopropylidene substitution increases activity and selectivity of biphenylmethylene 4-pyridine type CYP17 inhibitors. *J. Med. Chem.* **2010**, *53*, 5049–5053.

(13) Kawamoto, T.; Mitsuuchi, Y.; Toda, K.; Yokoyama, Y.; Miyahara, K.; Miura, S.; Ohnishi, T.; Ichikawa, Y.; Nakao, K.; Imura, H.; Ulick, S.; Shizuta, Y. Role of steroid 11β-hydroxylase and steroid 18-hydroxylase in the biosynthesis of glucocorticoids and mineralocorticoids in humans. *Proc. Natl. Acad. Sci. U.S.A.* **1992**, *89*, 1458–1462.

(14) (a) Hahner, S.; Stuermer, A.; Kreissl, M.; Reiners, C.; Fassnacht, M.; Haenscheid, H.; Beuschlein, F.; Zink, M.; Lang, K.; Allolio, B.; Schirbel, A. [^{123}I]Iodometomidate for Molecular Imaging of Adrenocortical Cytochrome P450 Family 11B Enzymes. *J. Clin. Endocrinol. Metab.* **2008**, *93*, 2358–65. (b) Zolle, I. M.; Berger, M. L.; Hammerschmidt, F.; Hahner, S.; Schirbel, A.; Peric-Simov, B. New selective inhibitors of steroid 11β-hydroxylation in the adrenal cortex. Synthesis and structure−activity relationship of potent etomidate analogues. *J. Med. Chem.* **2008**, *51*, 2244–2253.

(15) Bassett, M. H.; Mayhew, B.; Rehman, K.; White, P. C.; Mantero, F.; Arnaldi, G.; Stewart, P. M.; Bujalska, I.; Rainey, W. E. Expression profiles for steroidogenic enzymes in adrenocortical disease. *J. Clin. Endocrinol. Metab.* **2005**, *90*, 5446–5455.

(16) Taymans, S. E.; Pack, S.; Pak, E.; Torpy, D. J.; Zhuang, Z.; Stratakis, C. A. Human CYP11B2 (aldosterone synthase) maps to chromosome 8q24.3. *J. Clin. Endocrinol. Metab.* **1998**, *83*, 1033–1036.

(17) Ulmschneider, S.; Müller-Vieira, U.; Mitrenga, M.; Hartmann, R. W.; Oberwinkler-Marchais, S.; Klein, C. D.; Bureik, M.; Bernhardt, R.; Antes, I.; Lengauer, T. Synthesis and evaluation of imidazolylmethylenetetrahydronaphthalenes and imidazolylmethyleneindanes: Potent inhibitors of aldosterone synthase. *J. Med. Chem.* **2005**, *48*, 1796–1805.

(18) Ulmschneider, S.; Müller-Vieira, U.; Klein, C. D.; Antes, I.; Lengauer, T.; Hartmann, R. W. Synthesis and evaluation of (pyridylmethylene)tetrahydronaphthalenes/-indanes and structurally modified derivatives: potent and selective inhibitors of aldosterone synthase. *J. Med. Chem.* **2005**, *48*, 1563–1575.

(19) Voets, M.; Antes, I.; Scherer, C.; Müller-Vieira, U.; Biemel, K.; Barassin, C.; Oberwinkler-Marchais, S.; Hartmann, R. W. Heteroaryl substituted naphthalenes and structurally modified derivatives: selective inhibitors of CYP11B2 for the treatment of congestive heart failure and myocardial fibrosis. *J. Med. Chem.* **2005**, *48*, 6632–6642.

(20) Lucas, S.; Heim, R.; Negri, M.; Antes, I.; Ries, C.; Schewe, K. E.; Bisi, A.; Gobbi, S.; Hartmann, R. W. Novel aldosterone synthase inhibitors with extended carbocyclic skeleton by a combined ligand-based and structure-based drug design approach. *J. Med. Chem.* **2008**, *51*, 6138–6149.

(21) Voets, M.; Antes, I.; Scherer, C.; Müller-Vieira, U.; Biemel, K.; Oberwinkler-Marchais, S.; Hartmann, R. W. Synthesis and evaluation of heteroaryl-substituted dihydronaphthalenes and indenes: Potent and selective inhibitors of aldosterone synthase (CYP11B2) for the treatment of congestive heart failure and myocardial fibrosis. *J. Med. Chem.* **2006**, *49*, 2222–2231.

(22) (a) Belkina, N. V.; Lisurek, M.; Ivanov, A. S.; Bernhardt, R. Modelling of three-dimensional structures of cytochromes P450 11B1 and 11B2. *J. Inorg. Biochem.* **2001**, *87*, 197–207. (b) Lewis, D. F. V.; Lee-Robichaud, P. Molecular modelling of steroidogenic cytochromes P450 from families CYP11, CYP17, CYP19 and CYP21 based on the CYP102 crystal structure. *J. Steroid Biochem. Mol. Biol.* **1998**, *66*, 217–233. (c) Krone, N.; Riepe, F. G.; Götze, D.; Korsch, E.; Rister, M.; Commentz, J.; Partsch, C.-J.; Grötzinger, J.; Peter, M.; Sippell, W. G. Congenital adrenal hyperplasia due to 11-hydroxylase deficiency: functional characterization of two novel point mutations and a three-base pair deletion in the CYP11B1 gene. *J. Clin. Endocrinol. Metab.* **2005**, *90*, 3724–3730. (d) Roumen, L. L.; Sanders, M. P. A.; Koen, P.; Hilbers, P. A. J.; Plate, R.; Custers, E.; de Gooyer, M.; Smits, J. F. M.; Beugels, I.; Emmen, J.; Ottenheijm, H. C. J.; Leysen, D.; Hermans, J. J. R. Construction of 3D models of the CYP11B family as a tool to predict ligand binding characteristics. *J. Comput.-Aided Mol. Des.* **2007**, *21*, 455–471.

(23) Ulmschneider, S.; Negri, M.; Voets, M.; Hartmann, R. W. Development and evaluation of a pharmacophore model for inhibitors of aldosterone synthase (CYP11B2). *Bioorg. Med. Chem. Lett.* **2006**, *16*, 25–30.

(24) Crabb, T. A.; Soilleux, S. L. Microbiological transformations. Part 9: Microbiological transformations of 1,2,5,6-tetrahydropyrrolo-[3,2,1-*i,j*]-quinolin-4-one and of derivatives of 1,2,3,5,6,7-hexahydropyrido[3,2,1-*i,j*]quinoline with the fungus Cunninghamella elegans. *Tetrahedron* **1986**, *42*, 5407–5413.

(25) Appukkuttan, P.; Orts, A. B.; Chandran, R., P.; Goeman, J. L.; van der Eycken, J.; Dehaen, W.; van der Eycken, E. Generation of a small library of highly electron-rich 2-(hetero)aryl-substituted phenethylamines by the Suzuki−Miyaura reaction: a short synthesis of an apogalanthamine analogue. *Eur. J. Org. Chem.* **2004**, 3277–3285.

(26) Zhu, H.-F.; Zhao, W.; Okamura, T.; Fan, J.; Sun, W.-Y.; Ueyama, N. Syntheses and crystal structures of 1D tubular chains and 2D polycatenanes built from the asymmetric 1-(1-imidazolyl)-4-(imidazol-1-ylmethyl)benzene ligand with metal salts. *New J. Chem.* **2004**, *28*, 1010–1018.

(27) Ishiyama, T.; Murata, M.; Miyaura, N. Palladium(0)-catalyzed cross-coupling reaction of alkoxydiboron with haloarenes: a direct procedure for arylboronic esters. *J. Org. Chem.* **1995**, *60*, 7508–7510.

(28) Gotoh, O. Substrate recognition sites in cytochrome P450 family 2 (CYP2) proteins inferred from comparative analyses of amino acid and coding nucleotide sequences. *J. Biol. Chem.* **1992**, *267*, 83–90.

(29) (a) Mornet, E.; Dupont, J.; Vitek, A.; White, P. C. Characterization of two genes encoding human steroid 11β-hydroxylase [P-450(11)β]. *J. Biol. Chem.* **1989**, *264*, 20961–20967. (b) Kawamoto, T.; Mitsuuchi, Y.; Toda, K.; Miyahara, K.; Yokoyama, Y.; Nakao, K.; Hosoda, K.; Yamamoto, Y.; Imura, H.; Shizuta, Y. Cloning of cDNA and genomic DNA for human cytochrome P-45011β. *FEBS Lett.* **1990**, *296*, 345–349. (c) Kawamoto, T.; Mitsuuchi, Y.; Ohnishi, T.; Ichikawa, Y.; Yokoyama, Y.; Sumimoto, H.; Toda, K.; Miyahara, K.; Kuribayashi, I.; Nakao, K. Cloning and expression of a cDNA for human cytochrome P-450aldo as related to primary aldosteronism. Biochem. *Biophys. Res. Commun.* **1990**, *173*, 309–316.

(30) (a) Böttner, B.; Schrauber, H.; Bernhardt, R. Engineering a mineralocorticoid- to a glucocorticoid-synthesizing cytochrome P450. *J. Biol. Chem.* **1996**, *271*, 8028–8033. (b) Böttner, B.; Bernhardt, R. Changed ratios of glucocorticoid/mineralocorticoids caused by point mutations in the putative I-helix regions of CYP11B1 and CYP11B2. *Endocr. Res.* **1996**, *22*, 455–561. (c) Curnow, K. M.; Mulatero, P.; Emeric-Blanchouin, N.; Aupetit-Faisant, B.; Corvol, P.; Pascoe, L. The amino acid substitutions Ser288Gly and Val320Ala convert the cortisol producing enzyme, CYP11B1, into an aldosterone producing enzyme. *Nature Struct. Biol.* **1997**, *4*, 32–35. (d) Mulatero, P.; Curnow, K. M.; Aupetit-Taisant, B.; Foekling, M. Recombinant CYP11B genes encode enzymes that can catalyze conversion of 11-deoxycortisol to cortisol, 18-hydroxycortisol, and 18-oxocortisol. *J. Clin. Endocinol. Metab.* **1998**, *83*, 3996–4001. (e) Böttner, B.; Denner, K.; Bernhardt, R. Conferring aldosterone synthesis to human CYP11B1 by replacing key amino acid residues with CYP11B2-specific ones. *Eur. J. Biochem.* **1998**, *252*, 458–466. (f) Bechtel, S.; Belkina, N.; Bernhardt, R. The effect of amino acid substitutions I112P, D147E and K152N in CYP11B2 on the catalytic activities of the enzyme. *Eur. J. Biochem.* **2002**, *269*, 1118–1127.

(31) Ghosh, D.; Griswold, J.; Erman, M.; Pangborn, W. Structural basis for androgen specificity and estrogen synthesis in human aromatase. *Nature* **2009**, *457*, 219–223.

(32) (a) Ksander, G. M.; Meredith, E.; Monovich, L. G.; Papillon, J.; Firooznia, F.; Hu, Q.-Y. Preparation of condensed imidazole derivatives for the inhibition of aldosterone synthase and aromatase. PCT Int. Appl. WO2007024945, 2007. (b) Papillon J.; Ksander, G. M; Hu, Q.-Y. Preparation of tetrahydroimidazo[1,5-*a*]pyrazine derivatives as aldosterone synthase and/or 11β-hydroxylase inhibitors. PCT Int. Appl. WO2007139992, 2007. (c) Hu, Q.-Y.; Ksander, G. M. 4-Imidazolyl-1,2,3,4-tetrahydroquinoline derivatives and their use as aldosterone/11-beta-hydroxylase inhibitors. PCT Int. Appl. WO2008076860, 2008. (d) Hu, Q.-Y.; Ksander, G. M. Organic compounds. PCT Int. Appl. WO2008076862, 2008.

(33) Lucas, S.; Heim, R.; Ries, C.; Schewe, K. E.; Birk, B.; Hartmann, R. W. In vivo active aldosterone synthase inhibitors with improved selectivity: lead optimization providing a series of pyridine substituted 3,4-dihydro-1*H*-quinolin-2-one derivatives. *J. Med. Chem.* **2008**, *51*, 8077–8087.

(34) Ries, C.; Lucas, S.; Heim, R.; Birk, B.; Hartmann, R. W. Selective aldosterone synthase inhibitors reduce aldosterone formation in vitro and in vivo. *J. Steroid Biochem. Mol. Biol.* **2009**, *116*, 121–126.

(35) (a) Hartmann, R. W.; Heim, R., Lucas, S. 6-Pyridin-3-yl-3,4-dihydo-1*H*-quinoline-2-one derivatives and related compounds as inhibitors of the human aldosterone synthase CYP11B2. PCT Int. Appl. WO2009135651, 2009. (b) Hu, Q.; Hartmann, R. W. Unpublished results.

(36) (a) Denner, K.; Bernhardt, R. Inhibition studies of steroid conversions mediated by human CYP11B1 and CYP11B2 expressed in cell cultures. In *Oxygen Homeostasis and Its Dynamics*, 1st ed.; Ishimura, Y., Shimada, H., Suematsu, M., Eds.; Springer-Verlag: Tokyo, Berlin, Heidelberg, NY, 1998; pp 231−236. (b) Denner, K.; Doehmer, J.; Bernhardt, R. Cloning of CYP11B1 and CYP11B2 from normal human adrenal and their functional expression in COS-7 and V79 chinese hamster cells. *Endocr. Res.* **1995**, *21*, 443–448.

(37) Lamberts, S. W.; Bruining, H. A.; Marzouk, H.; Zuiderwijk, J.; Uitterlinden, P.; Blijd, J. J.; Hackeng, W. H.; de Jong, F. H. The new aromatase inhibitor CGS-16949A suppresses aldosterone and cortisol production by human adrenal cells in vitro. *J. Clin. Endocrinol. Metab.* **1989**, *69*, 896–901.

(38) Demers, L. M.; Melby, J. C.; Wilson, T. E.; Lipton, A.; Harvey, H. A.; Santen, R. J. The effects of CGS 16949A, an aromatase inhibitor on adrenal mineralocorticoid biosynthesis. *J. Clin. Endocrinol. Metab.* **1990**, *70*, 1162–1166.

(39) Heim, R.; Lucas, S.; Grombein, C. M.; Ries, C.; Schewe, K. E.; Negri, M.; Müller-Vieira, U.; Birk, B.; Hartmann, R. W. Overcoming undesirable CYP1A2 inhibition of pyridylnaphthalene type aldosterone synthase inhibitors: influence of heteroaryl derivatization on potency and selectivity. *J. Med. Chem.* **2008**, *51*, 5064–5074.

(40) Hille, U. E.; Zimmer, C.; Vock, C. A.; Hartmann, R. W. First selective CYP11B1 inhibitors for the treatment of cortisol-dependent diseases. *Med. Chem. Lett.* **2011**, *2*, 2–6.

(41) (a) Ehmer, P. B.; Jose, J.; Hartmann, R. W. Development of a simple and rapid assay for the evaluation of inhibitors of human 17α-hydroxylase-$C_{17,20}$-lyase (P450c17) by coexpression of P450c17 with NADPH-cytochrome-P450-reductase in *Escherichia coli*. *J. Steroid Biochem. Mol. Biol.* **2000**, *75*, 57–63. (b) Hutschenreuter, T. U.; Ehmer, P. B.; Hartmann, R. W. Synthesis of hydroxy derivatives of highly potent nonsteroidal CYP17 inhibitors as potential metabolites and evaluation of their activity by a noncellular assay using recombinant enzyme. *J. Enzyme Inhib. Med. Chem.* **2004**, *19*, 17–32.

(42) Thompson, E. A.; Siiteri, P. K. Utilization of oxygen and reduced nicotinamide adenine dinucleotide phosphate by human placental microsomes during aromatization of androstenedione. *J. Biol. Chem.* **1974**, *249*, 5364–5372.

(43) Molecular Operating Environment MOE 2009.10; CCGIM: Quebec, Canada, 2008; http://www.chemcomp.com

(44) Notredame, C.; Higgins, D.; Heringa, J. T-Coffee: A novel method for fast and accurate multiple sequence alignment. *J. Mol. Biol.* **2000**, *302*, 205–217.

(45) Cole, C.; Barber, J. D.; Barton, G. J. The JPRED 3 Secondary structure prediction server. *Nucleic Acids Res.* **2008**, *36*, W197–W201.

(46) McGuffin, L. J.; Bryson, K.; Jones, D. T. The PSIPRED protein structure prediction server. *Bioinformatics* **2000**, *16*, 404–405.

(47) Eswar, N.; Marti-Renom, M. A.; Webb, B.; Madhusudhan, M. S.; Eramian, D.; Shen, M.; Pieper, U.; Sali, A. *Current Protocols in Bioinformatics*, John Wiley & Sons, Inc.: New York, 2006.

(48) Laskowski, R. A.; MacArthur, M. W.; Moss, D. S.; Thornton, J. M. PROCHECK: a program to check the stereochemical quality of protein structures. *J. Appl. Crystallogr.* **1993**, *26*, 283–291.

(49) Wiederstein, M.; Sippl, M. J. ProSA-web: interactive web service for the recognition of errors in three-dimensional structures of proteins. *Nucleic Acids Res.* **2007**, *35*, W407–W410.

(50) Sippl, M. J. Recognition of Errors in Three-Dimensional Structures of Proteins. *Proteins* **1993**, *17*, 355–362.

(51) Kramer, B.; Rarey, M.; Lengauer, T. Evaluation of the FlexX incremental construction algorithm for protein−ligand docking. *Proteins: Struct., Funct., Genet.* **1999**, *37*, 228–241.